Hydrothermal conversion of FAU zeolite into RUT zeolite in TMAOH system

Hery Jon, Shoutarou Takahashi, Hitoshi Sasaki, Yasunori Oumi and Tsuneji Sano*

Department of Applied Chemistry, Graduate School of Engineering, Hiroshima University, Higashi-Hiroshima 739-8527, Japan; E-mail: tsano@hiroshima-u.ac.jp

Abstract

The highly crystalline and pure RUT (RUB-10) zeolite could be obtained from the hydrothermal conversion of FAU zeolite used as a crystalline Si/Al source in tetramethylammonium hydroxide (TMAOH) media. As compared to amorphous silica/$Al(OH)_3$ and amorphous silica/γ-Al_2O_3 sources, the crystallization rate for the formation of RUT zeolite was clearly faster when FAU zeolite was employed as the Si/Al source. Moreover, it was found that the hydrothermal conversion of FAU zeolite into RUT zeolite depended significantly upon the Si/Al ratio of the starting FAU zeolite. FAU zeolite could be hydrothermally converted into the highly crystalline and pure RUT zeolite under the following molar ratios: Si/Al = 17-28, $TMAOH/SiO_2$ = 0.2 and H_2O/SiO_2 = 3-7.

Keywords: FAU zeolite; RUT zeolite; Tetramethylammonium hydroxide; Hydrothermal conversion.

1. Introduction

Before the framework type was assigned to be RUT zeolite by IZA [1] based on the work of Gies et al. [2], the zeolite had been known as Nu-1 (*n*omenclature- *u*nknown-1) zeolite. The synthesis of aluminosilicate Nu-1 zeolite was reported in detail for the first time by Whittam et al. in 1977 [3]. It was claimed that Nu-1 zeolite has Si/Al ratio of 10 to 75 and that its H-form shows high activity and selectivity for xylenes isomerization. The hydrothermal synthesis was performed in the presence of tetramethylammonium (TMA) cations as organic structure-directing agent (OSDA). After this disclosure, the attempts to extend synthesis area yielded the remarkable achievement through the synthesis of boron isomorphous substituted Nu-1 zeolite (B-Nu-1) [4]. Moreover, in 1990 Bellussi et al. reported the possibility of synthesizing Nu-1 zeolite-like materials with boro-, gallo-, ferro- and aluminosilicate frameworks using TMAOH in the presence and absence of Na^+ cations [5]. In near-neutral fluoride containing media, Patarin et al. succeeded in the preparation of pure aluminosilicate Nu-1 zeolite even in a very narrow range of experimental conditions [6]. Almost two decades after Nu-1 zeolite was discovered, however, the crystal structure had remained unrevealed due to its microcrystallinity and poor crystallinity. In 1995 Gies et al. described the detailed ab initio analysis and the refinement of the crystal structure of RUB-10 (RUT) zeolite, a borosilicate Nu-1 zeolite, from low resolution powder X-ray diffraction data using Patterson search methods in combination with chemical analysis and physical characterization [2]. At the same year by the use of synchrotron powder diffraction data Broach et al. determined the structure of TMA silicate that has a chemical composition and XRD pattern similar to that of Nu-1 zeolite [7]. Furthermore, Ahedi et al. [8] and

Bhaumik et al. [9] described the synthesis of titanium substituted Nu-1 zeolite. Although the pure phase of all silica Nu-1 zeolite could not be obtained, Marler et al. [10] published the preparation of it by using pyrrolidine as OSDA instead of TMAOH (a well-known OSDA for RUT) in the presence of ammonium fluoride. From the above reports, moreover, it seems that in general the synthesis of RUT zeolite favors either the media containing Na^+ cations or high synthesis temperatures (150 – 180°C). Despite such system, in order to obtain the highly crystalline and pure RUT zeolite the synthesis commonly requires prolonged crystallization time.

Recently, the hydrothermal conversion of one zeolite into another, i.e. inter-zeolite conversion has drawn a lot of attention as an alternative synthesis strategy for zeolite synthesis [11-14]. Zones et al. reported that by the use of boron beta zeolite inter-zeolite conversion demonstrates enhanced nucleation, increased reaction rates and greater flexibility in choice of template and new possibilities for lattice substitution. Furthermore, it is believed that the crystalline starting material reduces supersaturation level and may have different surface reactivity for the generation of heterogeneous nucleation sites [11]. However, a detailed crystallization process (i.e. any evidence for an entity bringing about the above phenomena) during inter-zeolite conversion has not been clarified yet.

We have also investigated the potential of the hydrothermal conversion method, and very recently have reported the hydrothermal conversion of FAU zeolite into *BEA zeolite [15]. It was found that when the amount of tetraethylammonium hydroxide (TEAOH) added as OSDA is small, the crystallization rate toward *BEA zeolite from FAU zeolite is obviously faster than that from amorphous silica/γ-Al_2O_3. We supposed that the hydrothermal conversion route is of an alternative strategy for synthesizing

zeolite. In the present study, we investigated the possibility of zeolite synthesis with different zeolite frameworks using several OSDAs and succeeded in the hydrothermal conversion of FAU zeolite into highly crystalline and pure RUT zeolite in TMAOH media. The influences of hydrothermal conversion parameters on RUT zeolite synthesis are discussed in detail.

2. Experimental

2.1. Hydrothermal conversion

FAU zeolites with various Si/Al ratios used in this work were prepared from NH_4-Y zeolite (Si/Al = 2.8, Tosoh Co., Japan) through dealumination treatment involving a combination of steaming at 700°C and H_2SO_4 (0.74 – 0.85 M) treatment at 75°C for 4 h. The particle size of dealuminated FAU zeolite was 0.4 – 0.8 μm. The hydrothermal conversion was performed as follows. The dealuminated FAU zeolite was mixed well with aqueous TMAOH 20 wt% (Aldrich, USA) and then the mixture was placed into 30 cm^3 Teflon-lined stainless steel autoclave. The hydrothermal conversion was conducted at 140°C for 6 h – 18 days in the convection oven. The solid product was collected by centrifugation and washed thoroughly with deionized water until near neutral and then dried overnight at 70°C. For comparison, the starting gels from amorphous silica powder produced by wet process (SiO_2 = 88 wt%, Al_2O_3 = 0.27 wt%, Nipsil, Nippon Silica Ind. Japan) and sodium aluminate ($NaAlO_2$, Na_2O = 31-35 wt%, Al_2O_3 = 34-39 wt%, Kanto Chemical Co., Inc. Japan), $Al(OH)_3$ (Wako Pure Chemical Industries, Ltd.

Japan) or γ-Al_2O_3 (Catalysts & Chemicals Ind. Co., Ltd. Japan) as other Si and Al sources respectively were also prepared.

2.2. Characterization

The X-ray diffraction (XRD) patterns of the solid products were collected by powder X-ray diffractometer (Rigaku, RINT 2000) with graphite monochromatized Cu K_α radiation at 40 kV and 30 mA. The relative crystallinities of samples were calculated in relation to that of sample obtained after 6 days of heating. The crystallinity was based on the sum of intensities of peaks with reflection (-111), (111), (220), (022) and (-113). Si/Al ratios were determined by X-ray fluorescence (XRF, Philips spectrometer PW 2400). 0.5 g of sample was fused with 5 g of dilithium tetraborate ($Li_2B_4O_7$) at 1100°C. The Si/Al ratio was calculated by using Si and Al concentrations determined by the corresponding calibration curves. This Si/Al ratio accuracy has been confirmed by inductively-coupled plasma optical emission spectroscopy (ICP-OES, Seiko SPS 7700). The crystal morphology was observed using scanning electron microscopy (SEM, JEOL JSM-6320FS). Thermal analysis was carried out using TG/DTA (SSC/5200 Seiko Instruments). The sample about 7 mg was heated in a flow of air (50 mL/min) at 10°C/min from room temperature to 800°C. ^{13}C CP/MAS NMR and ^{27}Al MAS NMR spectra were recorded using a 7 mm diameter zirconia rotor on Bruker Avance DRX-400 at 100.6 MHz and 104.3 MHz, respectively. The rotor was spun at 4 kHz for ^{13}C CP/MAS NMR and 9 kHz for ^{27}Al MAS NMR. The spectra were accumulated with 6.0 μs pulses, 25 s recycle delay and 1000 scans for ^{13}C CP/MAS NMR, and 2.3 μs, 1 s and 4000 scans for ^{27}Al MAS NMR. Glycine (H_2NCH_2COOH) and $Al(NO_3)_3 \cdot 9H_2O$

were used as chemical shift references for ^{13}C CP/MAS NMR and ^{27}Al MAS NMR, respectively. Prior to ^{27}Al MAS NMR measurement, the sample was moisture-equilibrated over a saturated solution of NH_4Cl for 24 h.

3. Results and discussion

At first, in order to study the influence of Si/Al ratio of the starting FAU zeolite on RUT zeolite synthesis, FAU zeolites with various Si/Al ratios were prepared by the dealumination treatment and subjected to the hydrothermal treatment. The hydrothermal conversion conditions are listed in detail in Table 1. Fig. 1 shows the XRD patterns of the starting FAU zeolites with various Si/Al ratios and the products obtained after the hydrothermal treatment for 6 days. From these results, it was found that although the hydrothermal conversion toward pure RUT zeolite strongly depended upon the Si/Al ratio of the starting FAU zeolite, which was similar to the crystallization of *BEA zeolite from FAU zeolite [15], the highly crystalline and pure RUT zeolite could be easily obtained without any impurity. As stated in the introduction section, the synthesis of RUT zeolite seems to be difficult because some zeolitic phases commonly coexist with RUT zeolite as impurities. However, by the present route even at moderate temperature (i.e. 140°C) and the absence of Na^+ cations, the highly crystalline and pure RUT zeolite could be obtained from FAU zeolites with Si/Al ratios of 17 – 28; while Si/Al ratios of 14 and 33 yielded RUT zeolite together with SOD (sodalite) zeolite (denoted by asterisk in Fig. 1(B)-a) and amorphous phase, respectively. Fig. 2 shows the SEM images of RUT zeolites obtained. After thorough observation, we could not find any crystals of the starting FAU zeolite. Only crystals of RUT zeolite with disk-like

morphology were observed. The disk-like morphology of RUT zeolite observed here agrees with the results reported by Hao et al. [16]. Taking into account the fact that the Si/Al ratio of RUT zeolite was almost consistent with that of the starting FAU zeolite (see below), these results strongly indicate that FAU zeolite was completely converted into RUT zeolite during hydrothermal treatment in TMAOH media. Moreover, from Table 1 it was observed that when the Si/Al ratios were 10 and 14, i.e. higher aluminum content, the formation of SOD zeolite considerably competed with RUT zeolite. It seems that high aluminum system favors the formation of SOD zeolite (see below).

In the case of the synthesis of *BEA zeolite from FAU zeolite, as the starting material from FAU zeolite showed faster crystallization rate toward *BEA zeolite, compared to amorphous silica/γ-Al_2O_3, we supposed that local-ordered aluminosilicate species (zeolitic building units) originated by the decomposition and dissolution of FAU zeolite framework under alkaline media of TEAOH may be present. We put forward the hypothesis based on the following considerations. To start with, Davis et al. who also studied the inter-zeolite conversion suggested a possibility of an existence of such aluminosilicates species, whose structure and concentration were affected by the framework type and composition of the starting zeolite [14]. Furthermore, Matsukata et al. [17] and Pinnavaia et al. [18] also showed the presence of aluminosilicate species by analyzing the mesoporous materials prepared using the solution obtained from the dissolution of ZSM-5 zeolite. Thus, in order to further support the hypothesis, we studied the crystallization kinetics of RUT zeolite with various Si/Al sources. The crystallization curves are presented in Fig. 3. It became clear that the crystallization rate toward RUT zeolite from FAU zeolite was obviously faster than that from amorphous silica/$Al(OH)_3$ and amorphous silica/γ-Al_2O_3 sources. To obtain highly crystalline RUT

zeolite, in the case of amorphous silica/$Al(OH)_3$ and amorphous silica/γ-Al_2O_3 sources the crystallization time required 15 and 18 days (Table 1, Sample nos. 18 and 19; Fig. 3), respectively; while for FAU zeolite source it only required 6 days. These data also seem to strongly support our hypothesis that the local-ordered aluminosilicate species originated by the decomposition and dissolution of FAU zeolite framework may exist and be taking part in the construction of another zeolite framework in the presence of a specific OSDA. Although the hypothesis only indirectly describes the phenomena, in order to obtain the direct evidence the thorough investigation is now in progress. The use of zeolite as an alternative Si/Al source therefore provides several advantages in the enhancement of crystallization rate and the description of synthesis mechanism. Moreover, for comparison with the system prepared under the presence of Na^+ cations, we also performed the synthesis involving sodium aluminate as aluminum source together with sodium source consequently. The result that the crystallization rate from this system is faster than that from FAU zeolite was observed (Fig. 3). It should be noted that because in this system there are additional hydroxide ions from sodium aluminate that is bringing about the gel more soluble and more reactive and thus enhancing crystallization rate, it is almost impossible to compare this system to that from FAU zeolites directly. However, the information which can be achieved here is that the use of FAU zeolite considerably enhances the crystallization rate and the enhancement is comparable to that with sodium aluminate.

Furthermore, other parameters involved in hydrothermal conversion such as temperature, H_2O/SiO_2 ratio and $TMAOH/SiO_2$ ratio were also investigated thoroughly. In Table 1 when the starting FAU zeolite with Si/Al ratio of 22 was subjected to hydrothermal treatment at 170°C, the crystalline RUT zeolite could be obtained even

after 2 days of heating (Sample no. 8). This phenomenon can be easily explained as follows; since with the increase of synthesis temperature the decomposition and dissolution rate of the starting FAU zeolite also remarkably increases, the assembly rate (i.e. nucleation rate) and the crystal growth rate of RUT zeolite increase as well. Fig. 4 shows XRD patterns of solid products obtained from FAU zeolites with various H_2O/SiO_2 ratios. It was found that in the range of H_2O/SiO_2 ratios of 3-7, the highly crystalline RUT zeolites without any impurity could be achieved with this route (Fig. 4, Sample nos. 6, 7 and 9). On the other hand, while the H_2O/SiO_2 ratio was 10, RUT zeolite along with amorphous phase was observed. This implies that more dilute system, namely less reactive, seems to be not favorable to the growth of RUT zeolite. Indeed, the more dilute system decreased the crystallization rate toward RUT zeolite. The SEM images of them are exhibited in Figs. 5 and 2(c). There was nearly no difference in the crystallites size and morphology even synthesized with different H_2O/SiO_2 ratios (3-7). Moreover, Fig. 6 shows the XRD patterns of samples obtained from FAU zeolites prepared with various $TMAOH/SiO_2$ ratios. It was clear that only $TMAOH/SiO_2$ ratio of 0.2 could transform FAU zeolite into highly crystalline and pure RUT zeolite (Fig. 6(b)), while $TMAOH/SiO_2$ ratios of 0.1, 0.3 and 0.4 produced a small amount of undissolved FAU zeolite together with amorphous phase, RUT zeolite coexisted with a small amount of SOD zeolite and SOD zeolite with a small amount of RUT zeolite, respectively (Figs. 6(a), (c) and (d)). These results can be explained as follows. When the amount of TMAOH is small ($TMAOH/SiO_2 = 0.1$), the alkalinity of system required to decompose or dissolve FAU zeolite decreases and thus are not enough to break up FAU zeolite completely. On the other hand, with the increase of amount of TMAOH the alkalinity also increases consequently. In the case of the synthesis of *BEA zeolite in

TEAOH media, it has been already recognized that in extremely high alkalinity the aluminum-core is more favorable than the silicon one [19-21]. Therefore, in the case of TMAOH, the similar argument can be deduced. However, because TMA^+ cations are well-known as OSDA for the synthesis of SOD zeolite, an aluminous clathrasil [22-24], the favorable aluminum core leads to the preferential formation of SOD zeolite. Sample nos. 2 and 3 in Table 1 also supported this argument.

Moreover, the subsequent analyses were conducted in order to get information concerning the characteristics of RUT zeolite obtained by the hydrothermal conversion of FAU zeolite. The characteristics of organic molecules occluded in the pores were characterized by thermal analysis and ^{13}C CP/MAS NMR spectroscopy. The TG/DTA curves corresponding to Sample no. 7 are presented in Fig. 7. From the DTA curve, we can categorize thermal profiles into five zones: (I) 25-200°C, (II) 200-350°C, (III) 350-500°C, (IV) 500-700°C and (V) 700-800°C. The first zone with endothermic profile corresponds to the desorption of adsorbed water. Then the second zone with exothermic profile centered at 250°C is attributed to the decomposition and oxidation of either TMAOH occluded in pores [24] or TMA^+ cations interacting with silanol groups of crystal defects. Next, the third zone with exothermic profile centered at 450°C is assigned to the decomposition and oxidation of TMA^+ cations balancing the negative charge of framework generated by Al [25,26]. The forth zone with exothermic profile centered at 600°C corresponds to the decomposition and oxidation of either hydrocarbon residue produced on acid sites or pyrolysis products in the former steps. The fifth zone with a slightly endothermic profile indicates the dehydration through the condensation of silanol groups [27], which seems likely to imply the structure collapse. Based on the profiles described above, the weight losses between 200 and 700°C that

are corresponding to the total decomposition of organic moieties are about 15.2 wt% (ca. 5 TMA^+/u.c.). Likewise, by ^{13}C CP/MAS NMR spectroscopy the nature of organic moieties was studied. Fig. 8 depicts ^{13}C CP/MAS NMR spectrum of Sample no. 7. The spectrum revealed the presence of 2 resonances which centered at 57.1 and 45.3 ppm. Resonance at 57.1 ppm indicates methyl groups attached to N, namely $–CH_3$ of $N(CH_3)^+$, while resonances at 45.3 ppm is corresponding to methylene groups of $N\text{-}CH_2\text{-}CH_3$ moieties [28], that are formed by the degradation of a small amount of TMAOH. It can be concluded that although there was a small amount of degraded TMA^+ species, almost all of TMA^+ species existed intact in zeolitic pores.

Furthermore, the chemical state of aluminum in the RUT zeolite obtained was investigated by elemental analysis and ^{27}Al MAS NMR spectroscopy. The elemental analyses were performed by XRF. According to the results listed in Table 1, the bulk Si/Al ratios of the products were almost consistent with those of starting FAU zeolites, indicating that almost all of aluminum species have been converted from FAU zeolites into RUT zeolites. Then, to clarify the chemical state of aluminum in the zeolite, ^{27}Al MAS NMR spectra of as-synthesized and calcined Sample no. 7 were measured. Fig. 9(a) exhibits the spectrum of the as-synthesized sample. Only two resonances centered at 57.6 and 52.2 ppm were observed, while no resonance corresponding to octahedrally coordinated aluminum species, namely extraframework aluminum species, at chemical shift of around 0 ppm was observed. This means that all of aluminum species which are present in RUT zeolite obtained from hydrothermal conversion of FAU zeolite exist within the zeolite framework. Furthermore, the observation of two resonances indicates the presence of at least two groups of crystallographically distinct T-sites in RUT zeolite framework. According to the crystallographic data in literature [1,2], RUT

zeolite consists of five different T-sites. Abraham et al. by ^{27}Al MAS NMR and ^{27}Al 3Q MAS NMR measurements also found the similar results in *BEA zeolite [29]. Yet, in the ^{27}Al MAS NMR spectrum of RUT zeolite calcined at 500°C for 10 h (Fig. 9(b)), the considerable decrease in the intensity of resonance for framework aluminum was observed, indicating severe dealumination.

4. Conclucions

The hydrothermal conversion parameters influencing the conversion of FAU zeolite into RUT zeolite in the presence of TMAOH were investigated in detail. As compared to amorphous silica/$Al(OH)_3$ and amorphous silica/γ-Al_2O_3 sources, the crystallization rate toward the formation of RUT zeolite was clearly faster when FAU zeolite was employed as Si and Al sources. It seems that the decomposition and the dissolution of FAU zeolite in TMAOH media serve local-ordered aluminosilicate species which readily build up RUT zeolite framework. Moreover, it was found that the hydrothermal conversion of FAU zeolite into RUT zeolite depended significantly upon the Si/Al ratio of the starting FAU zeolite. FAU zeolite could be hydrothermally converted into the highly crystalline and pure RUT zeolite under the following molar ratios: Si/Al = 17-28, $TMAOH/SiO_2$ = 0.2 and H_2O/SiO_2 = 3-7. By TG/DTA analysis the weight loss corresponding to the degradation of TMA^+ species was about 15.2 wt%. As confirmed by ^{13}C CP MAS NMR spectrum, almost all of TMA^+ species existed intact in zeolitic pores. In addition, ^{27}Al MAS NMR spectrum of as-synthesized RUT zeolite showed that tetrahedrally coordinated aluminum species could be resolved into at least two crystallographically distinct T-sites. The absence of octahedrally coordinated aluminum

species implied that all of aluminum species are present within the zeolitic framework before calcination.

References

[1] Ch. Baerlocher, W.M. Meier, D.H. Olson, Atlas of Zeolite Framework Types, 5th Ed., Elsevier, Amsterdam, 2001. Also in URL: http://web.iza-structure.org/databases/

[2] H. Gies, J. Rius, Z. Kristallogr. 210 (1995) 475.

[3] T.V. Whittam, B. Youll, US Patent 4 060 590, Imperial Chemical Industries Ltd., London, 1977.

[4] M. Taramasso, G. Perego, B. Notari, in L.V.C. Rees (Ed.), Proceedings of the Fifth International Conference on Zeolites, Naples, Heyden, London, 1980, pp. 40.

[5] G. Bellussi, R. Millini, A. Carati, G. Maddinelli, A. Gervasini, Zeolites 10 (1990) 642.

[6] J. Patarin, P. Caullet, B. Marler, A.C. Faust, J.L. Guth, Zeolites 14 (1994) 675.

[7] R.W. Broach, N.K. McGuire, C.C. Chao, R.M. Kirchner, J. Phys. Chem. Solids 56 (1995) 1363.

[8] R.K. Ahedi, S.S. Shevade, A.N. Kotasthane, Zeolites 18 (1997) 361.

[9] A. Bhaumik, T. Tatsumi, Micropor. Mesopor. Mater. 34 (2000) 1.

[10] B. Marler, U. Werthmann, H. Gies, Micropor. Mesopor. Mater. 43 (2001) 329.

[11] C.S. Cundy, P.A. Cox, Micropor. Mesopor. Mater. 82 (2005) 1 and references therein.

[12] S. Khodabandeh, M.E. Davis, Micropor. Mater. 9 (1997) 149.

[13] S. Khodabandeh, G. Lee, M.E. Davis, Micropor. Mater. 11 (1997) 87.

[14] S. Khodabandeh, M.E. Davis, Micropor. Mater. 12 (1997) 347.

[15] H. Jon, K. Nakahata, B.-W. Lu, Y. Oumi, T. Sano, Micropor. Mesopor. Mater. 96 (2006) 72.

[16] X. Hao, S. Liu, N. Guan, Stud. Surf. Sci. Catal. 154 (2004) 2275.

[17] S. Inagaki, M. Ogura, T. Inami, Y. Sasaki, E. Kikuchi, M. Matsukata, Micropor. Mesopor. Mater. 74 (2004) 163.

[18] H. Wang, Y. Liu, T.J. Pinnavaia, J. Phys. Chem. B 110 (2006) 4525.

[19] M.A. Camblor, A. Corma, A. Mifsud, J. Pérez-Pariente, S. Valencia, Stud. Surf. Sci. Catal. 105 (1997) 341.

[20] S. Mintova, V. Valtchev, T. Onfroy, C. Marichal, H. Knözinger, T. Bein, Micropor. Mesopor. Mater. 90 (2006) 237.

[21] H. Jon, Y. Oumi, K. Itabashi, T. Sano, J. Cryst. Growth. 307 (2007) 177.

[22] R.F. Lobo, S.I. Zones, M.E. Davis, J. Inclus. Phenom. Mol. 21 (1995) 47.

[23] R.M. Barrer, Hydrothermal Chemistry of Zeolites, Academic Press, London, 1982, p. 162.

[24] Ch. Baerlocher, W.M. Meier, Helv. Chim. Acta 52 (1969) 1853.

[25] E. Bourgeat-Lami, F. Di Renzo, F. Fajula, P.H. Mutin, T.D. Courieres, J. Phys. Chem. 96 (1992) 3807.

[26] M.A. Camblor, A. Corma, S. Valencia, J. Mater. Chem. 8 (1998) 2137.]

[27] Y.X. Wang, H. Gies, J.H. Lin, Chem. Mater. 19 (2007) 4181.

[28] C.J. Pouchert, J. Behnke, The Aldrich Library of ^{13}C and ^{1}H FT NMR Spectra, Aldrich Chemical Co. Inc., USA, 1993.

[29] A. Abraham, S.-H. Lee, C.-H. Shin, S.B. Hong, R. Prins, J.A. van Bokhoven, Phys. Chem. Chem. Phys. 6 (2004) 3031.

Figure captions

Fig. 1. XRD patterns of (A) the starting FAU zeolites with various Si/Al ratios and (B) the products obtained after hydrothermal treatment. Sample nos.: (a) 3, (b) 4, (c) 7, (d) 13 and (e) 14. The asterisk mark denotes the peak of SOD (sodalite) zeolite that is present as impurity.

Fig. 2. SEM images of (a) the starting FAU zeolite with Si/Al ratio of 22 and the RUT zeolites obtained from FAU zeolites with various Si/Al ratios. Sample nos.: (b) 4, (c) 7 and (d) 13.

Fig. 3. Crystallization curves of the RUT zeolites prepared from (◆) FAU zeolite, (●) amorphous silica/$NaAlO_2$, (▲) amorphous silica/$Al(OH)_3$ and (■) amorphous silica/γ-Al_2O_3 under hydrothermal conditions: Si/Al = 22, $TMAOH/SiO_2$ = 0.2 and H_2O/SiO_2 = 5 at 140°C.

Fig. 4. XRD patterns of the RUT zeolites obtained from FAU zeolites with various H_2O/SiO_2 ratios. Sample nos.: (a) 6, (b) 7, (c) 9 and (d) 10.

Fig. 5. SEM images of the RUT zeolites obtained from FAU zeolites with various H_2O/SiO_2 ratios. Sample nos.: (a) 6 and (b) 9.

Fig. 6. XRD patterns of the RUT zeolites obtained from FAU zeolites with various $TMAOH/SiO_2$ ratios. Sample nos.: (a) 5, (b) 7, (c) 11 and (d) 12.

Fig. 7. TG/DTA curves of sample no. 7.

Fig. 8. ^{13}C CP MAS NMR spectrum of sample no. 7.

Fig. 9. ^{27}Al MAS NMR spectra of (a) as-synthesized and (b) calcined sample no. 7.

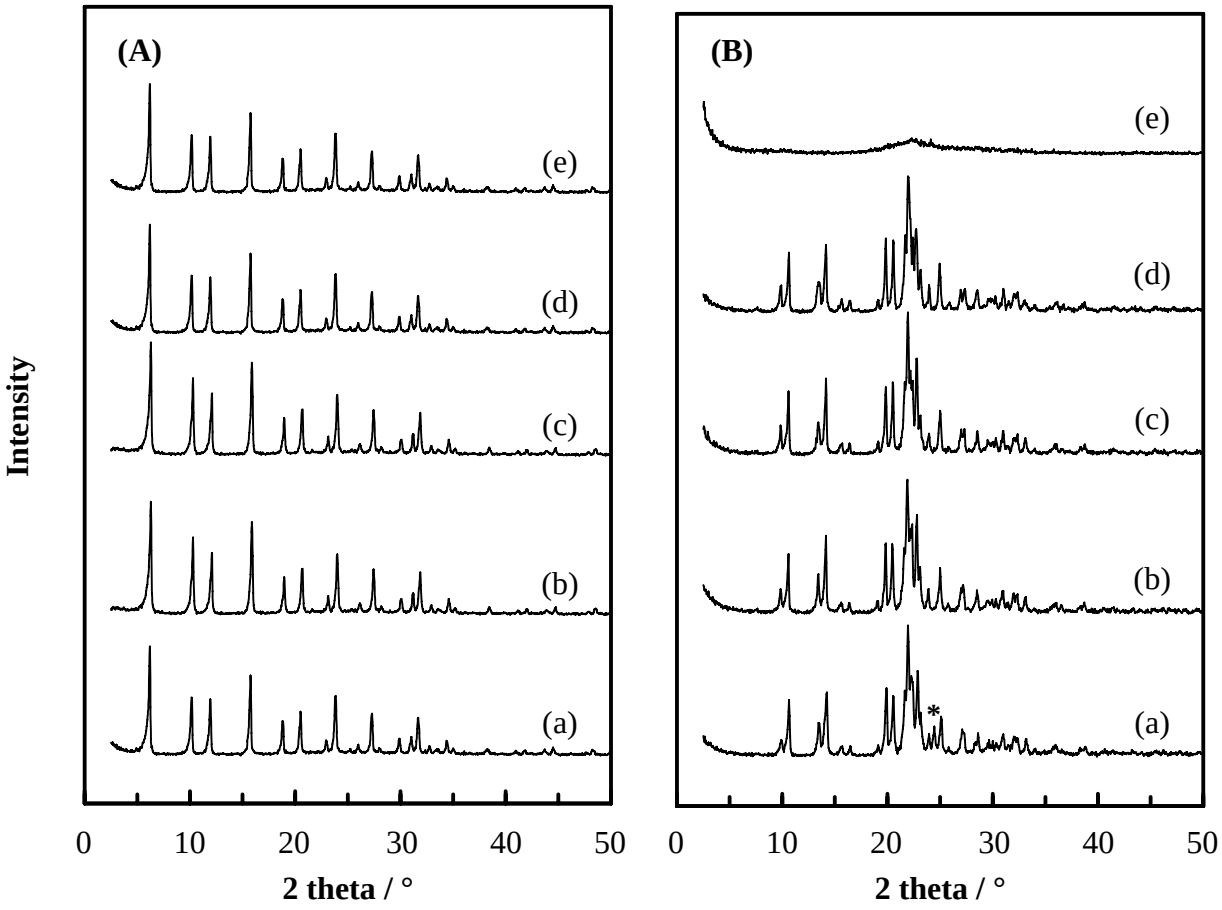

Figure 1

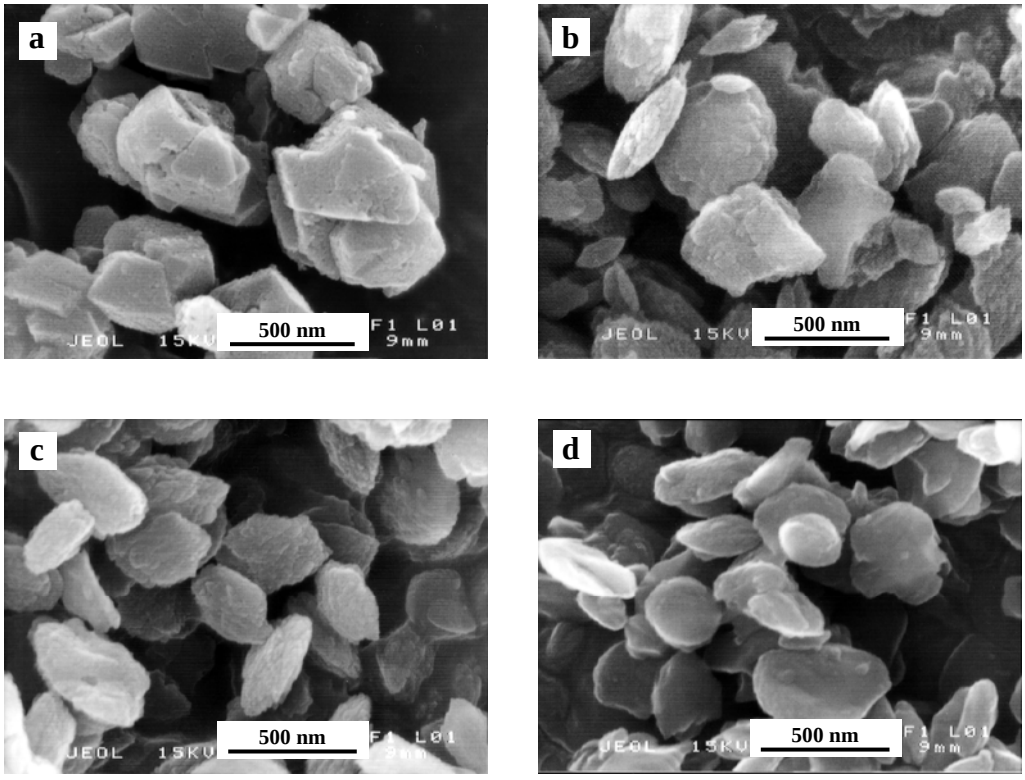
a
500 nm
JEOL 15KV F1 L01 9mm
b
500 nm
JEOL 15KV F1 L01 9mm
c
500 nm
d
500 nm
JEOL 15KV F1 L01 9mm

Figure 2

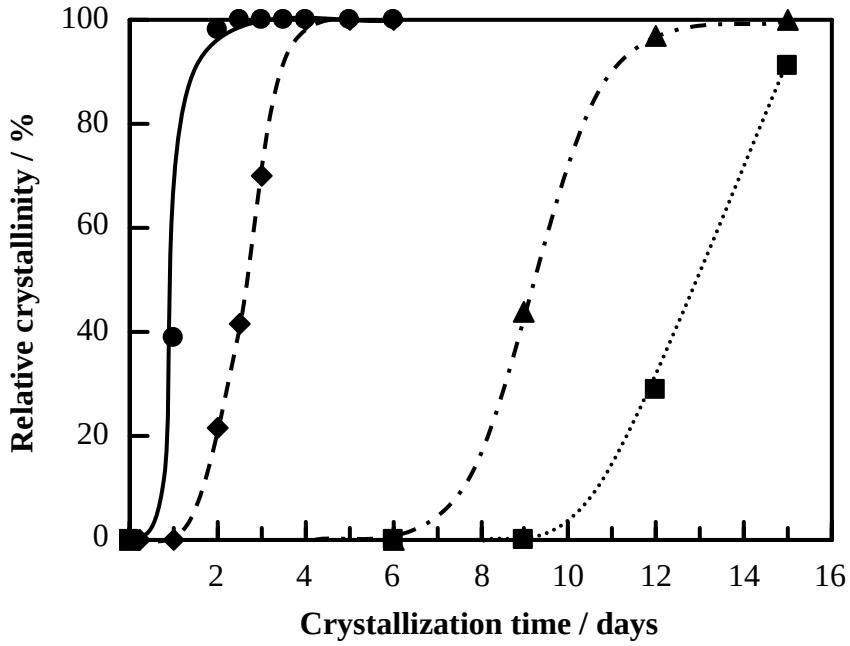
Relative crystallinity / %
100
80
60
40
20
0
2
4
6
8
10
12
14
16
Crystallization time / days

Figure 3

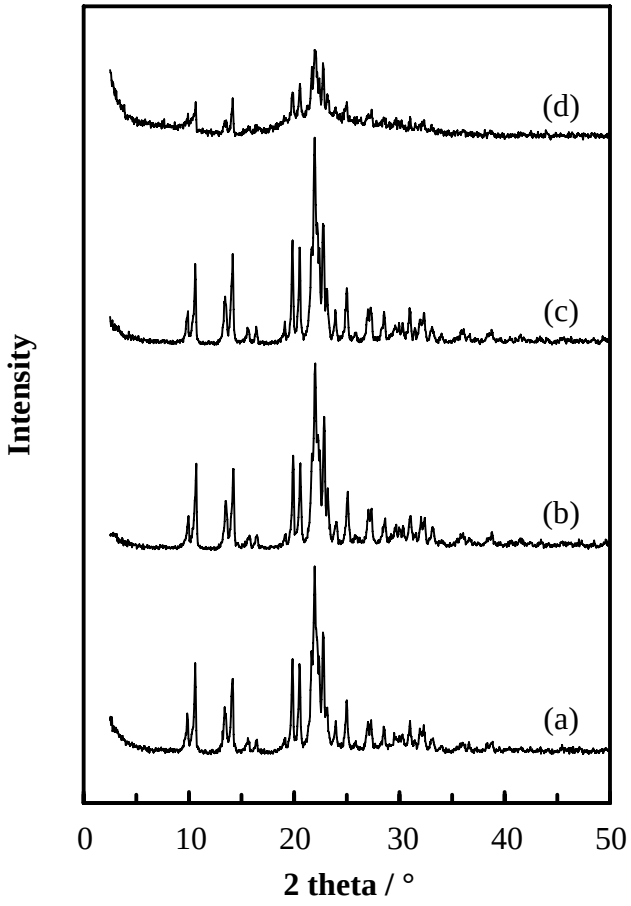

Figure 4

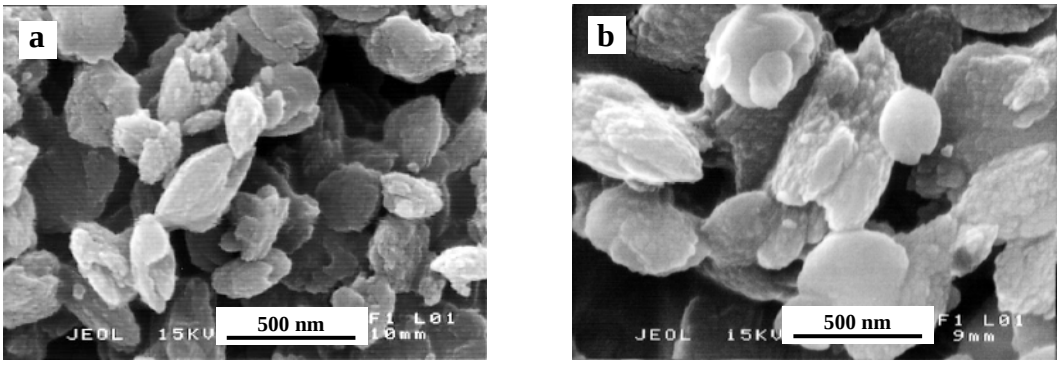

Figure 5

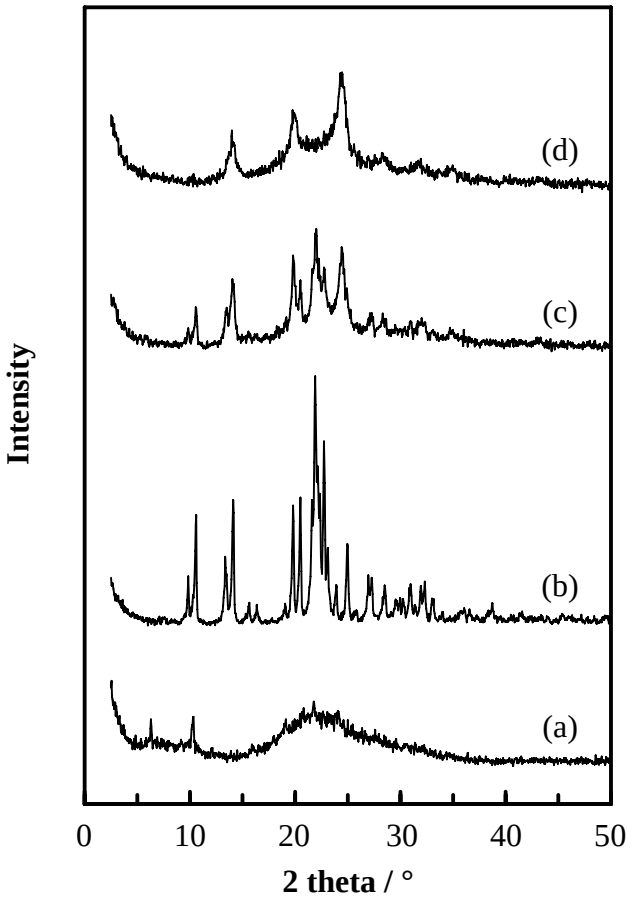

Figure 6

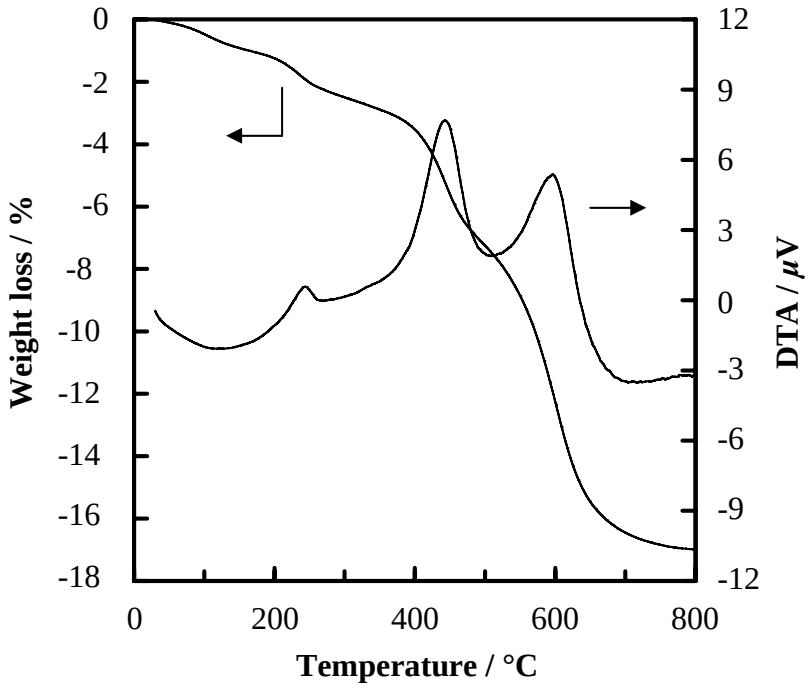
0
-2
-4
-6
-8
-10
-12
-14
-16
-18
Weight loss / %
12
9
6
3
0
-3
-6
-9
-12
DTA / μV
0
200
400
600
800
Temperature / °C

Figure 7

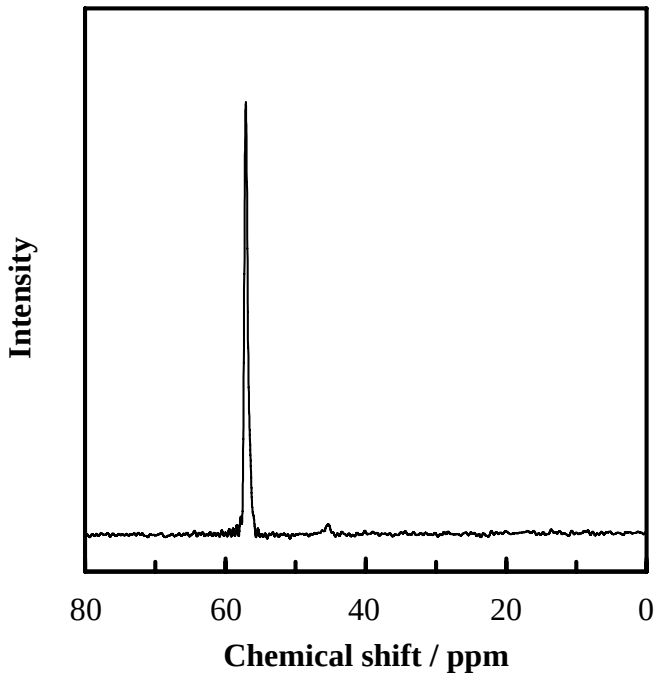

Figure 8

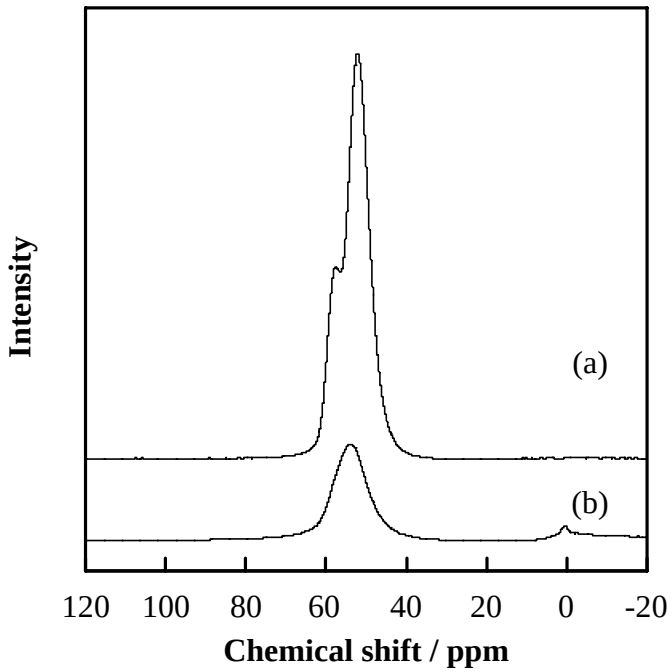

Figure 9

Table 1
Hydrothermal conversion conditions and products obtained

Sample no.	Synthesis conditions						Product (by product)	
	Si and Al sources	Si/Al ratio	TMAOH/ SiO_2	H_2O/ SiO_2	Temp. / °C	Time / days	Phase[a]	Bulk Si/Al ratio
1	FAU	3	0.2	5	140	6	FAU	
2	FAU	10	0.2	5	140	6	RUT (SOD)	
3	FAU	14	0.2	5	140	6	RUT (SOD)	
4	FAU	17	0.2	5	140	6	RUT	17
5	FAU	22	0.1	5	140	6	AM (FAU)	
6	FAU	22	0.2	3	140	6	RUT	
7	FAU	22	0.2	5	140	6	RUT	20
8	FAU	22	0.2	5	170	2	RUT	21
9	FAU	22	0.2	7	140	6	RUT	21
10	FAU	22	0.2	10	140	6	RUT (AM)	21
11	FAU	22	0.3	5	140	6	RUT (SOD)	
12	FAU	22	0.4	5	140	6	SOD (RUT)	
13	FAU	28	0.2	5	140	6	RUT	28
14	FAU	33	0.2	5	140	6	AM	
15	FAU	50	0.2	5	140	6	AM	
16	SiO_2 + $Al(OH)_3$	22	0.2	5	140	6	AM	
17	SiO_2 + γ-Al_2O_3	22	0.2	5	140	6	AM	
18	SiO_2 + $Al(OH)_3$	22	0.2	5	140	15	RUT	21
19	SiO_2 + γ-Al_2O_3	22	0.2	5	140	18	RUT	21
20	SiO_2 + $NaAlO_2$	22	0.2	5	140	2	RUT	21

[a] RUT = RUB-10, SOD = Sodalite, FAU = Faujasite, AM = Amorphous